

MIT Open Access Articles

Atmospheric evolution of volcanic smog ("vog") from Kilauea: Real-time measurements of oxidation, dilution, and neutralization within a volcanic plume

The MIT Faculty has made this article openly available. **Please share** how this access benefits you. Your story matters.

Citation: Kroll, Jesse H., Eben S. Cross, James F. Hunter, Sidhant Pai, Lisa M. M. Wallace, Philip L. Croteau, John T. Jayne, et al. "Atmospheric Evolution of Sulfur Emissions from Kilauea: Real-Time Measurements of Oxidation, Dilution, and Neutralization Within a Volcanic Plume." *Environ. Sci. Technol.* 49, no. 7 (April 7, 2015): 4129–4137.

As Published: <http://dx.doi.org/10.1021/es506119x>

Publisher: American Chemical Society (ACS)

Persistent URL: <http://hdl.handle.net/1721.1/101870>

Version: Author's final manuscript: final author's manuscript post peer review, without publisher's formatting or copy editing

Terms of Use: Article is made available in accordance with the publisher's policy and may be subject to US copyright law. Please refer to the publisher's site for terms of use.



1 **Atmospheric evolution of volcanic smog (“vog”) from Kīlauea:**

2 **Real-time measurements of oxidation, dilution, and neutralization within a volcanic plume**

3
4 Jesse H. Kroll*[†]#, Eben S. Cross[†]#, James F. Hunter[†], Sidhant Pai[†], TREX XII[†], TREX XI[†],
5 Lisa M. M. Wallace[‡], Philip L. Croteau[§], John T. Jayne[§], Douglas R. Worsnop[§], Colette L.
6 Heald[†], Jennifer G. Murphy[⊗], and Sheila L. Frankel[†]

7
8 [†] Department of Civil and Environmental Engineering, Massachusetts Institute of Technology,
9 Cambridge, MA, United States

10 [§] Center for Aerosol and Cloud Chemistry, Aerodyne Research, Inc., Billerica MA, United States

11 [‡] Air Surveillance and Analysis Section, Hawai‘i State Department of Health, Hilo, HI, United
12 States

13 [⊗] Department of Chemistry, University of Toronto, Toronto, ON, Canada

14
15
16 Members of TREX XII included Sara Comis, Brianna Coston, Flor De La Cruz, Michelle Dutt,
17 Amairani Garcia, Majdolene Khweis, Elaine Kung, Matthew Monheit, Theresa Oehmke, Jessica
18 Parker, Ricardo Ramos-Martin, Alexander Severt, and Phoebe Whitwell.

19 Members of TREX XI included Jhanel Chew, Kelley Determan, Di Jin, Anna Kelly, Zara
20 L’Heureux, Michelle Morales, Kelden Pehr, Marcela Rodriguez, Theresa Santiano-McHatton,
21 Tara Soni, Priscilla Soto, Iovana Valdez, Jibo Wen, Jaclyn Wilson, Eric Alm, Kelly Daumit,
22 Donald Frankel, and Janelle Thompson.

23
24
25 * To whom correspondence should be addressed: jhkroll@mit.edu , 617-253-2409.

26 # These authors contributed to this work equally.
27

28 **Atmospheric evolution of volcanic smog (“vog”) from Kilauea:**

29 **Real-time measurements of oxidation, dilution, and neutralization within a volcanic plume**

30
31 **Abstract.**

32 The high atmospheric concentrations of toxic gases, particulate matter, and acids in the areas
33 immediately surrounding volcanoes can have negative impacts on human and ecological health.
34 In order to better understand the atmospheric fate of volcanogenic emissions in the near field (in
35 the first few hours after emission), we have carried out real-time measurements of key chemical
36 components of the volcanic plume from Kīlauea on the Island of Hawai‘i. Measurements were
37 made at two locations, one ~3 km north-northeast of the vent and the other 31 km to the
38 southwest, with sampling at each site spanning a range of meteorological conditions and volcanic
39 influence. Instrumentation included a sulfur dioxide monitor and an Aerosol Chemical
40 Speciation Monitor, allowing for a measurement of the partitioning between the two major sulfur
41 species (gas-phase SO₂ and particulate sulfate) every 5 minutes. During trade wind conditions,
42 which sent the plume toward the southwest site, sulfur partitioning exhibited a clear diurnal
43 pattern, indicating photochemical oxidation of SO₂ to sulfate; this enabled the quantitative
44 determination of plume age (5 hours) and instantaneous SO₂ oxidation rate ($2.4 \times 10^{-6} \text{ s}^{-1}$ at solar
45 noon). Under stagnant conditions near the crater, the extent of SO₂ oxidation was substantially
46 higher, suggesting faster oxidation. The particles within the plume were extremely acidic, with
47 pH values (controlled largely by ambient relative humidity) as low as -0.8 and strong acidity
48 (controlled largely by absolute sulfate levels) up to 2200 nmol/m³. The high variability of sulfur
49 partitioning and particle composition underscores the chemically dynamic nature of volcanic
50 plumes, which may have important implications for human and ecological health.

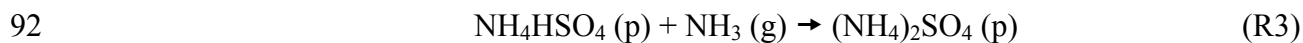
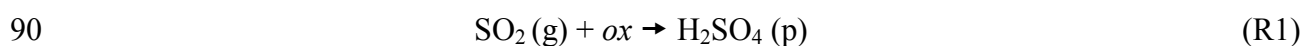
52 **Introduction.**

53 Volcanoes are a major source of sulfur to the atmosphere, accounting for ~20-40% of natural
54 sulfur emissions and ~10% of sulfur emissions overall.¹ Gaseous forms of volcanogenic sulfur
55 include sulfur dioxide (SO₂, 13.4 Tg/yr), hydrogen sulfide (H₂S, 2.8 Tg/yr), and other trace
56 species.² Particulate sulfate (SO₄²⁻) is also emitted directly from volcanoes,³ though most
57 volcanogenic sulfate is secondary, formed from the atmospheric oxidation of SO₂. Because of
58 the large impact that sulfate particles have on the radiative balance of the atmosphere, via direct
59 interactions with radiation as well as modification of cloud properties and lifetimes,⁴ much of the
60 focus on volcanoes in the atmospheric chemistry literature has been on quantifying their impact
61 on past and present climate. However, volcanic emissions can also have adverse impacts on
62 human and ecological health. It is estimated that over 450 million people worldwide live near
63 active volcanoes,⁵ and toxic volcanic gases and particulate matter therefore are likely to pose a
64 health hazard globally.^{6,7}

65 Within the United States, the dominant source of volcanic sulfur emissions is Kīlauea
66 Volcano on the Island of Hawai‘i. Kilauea currently emits ~1 Tg SO₂ per year;⁸ this is smaller
67 than anthropogenic SO₂ emissions in the U.S. (~6 Tg SO₂/yr⁹) but derives from a single point
68 source, and so can have major impacts on local health and ecology. The plume of volcanic
69 emissions (“volcanic smog”, or “vog”) is known in the area as a major nuisance, and has been
70 shown to have adverse cardiorespiratory health impacts on island residents.¹⁰⁻¹³ This has been
71 especially pronounced since March 2008, when a new vent opened in the Halema‘uma‘u crater
72 (see Figure S1), shifting the majority of the volcano’s emissions further inland, increasing the
73 vog exposure of local residents, and leading to exacerbated health effects.^{14,15} Since the
74 meteorology is dominated by strong trade winds, most of the time the Halema‘uma‘u plume

75 travels to the southwest, passing through communities such as Pahala (population 1,356).
76 Communities on the west coast (such as Kailua, population 11,975) can also be affected via
77 onshore/offshore winds. However at times (especially in the winter) the wind pattern can reverse,
78 with “Kona winds” sending the plume to the northeast, toward more populous areas such as Hilo
79 (population 43,263). Thus the Halema‘uma‘u plume has the potential to affect the health and
80 well-being of a large number of people living in the region.

81 The detailed impact of such volcanic emissions on human and ecological health is a
82 function of not only the plume’s intensity (which is controlled by emission rate and transport)
83 but also the relative abundance of various chemical species within the plume. Because of
84 chemical reactions that take place within the plume, the plume composition is highly dynamic,
85 ^{16,17} and dependent on a number of factors that vary with time and location (e.g., meteorological
86 conditions, sunlight, and local emissions). Such reactions will govern the amount and
87 composition of volcano-derived particulate matter; key reactions are the oxidation of SO₂ to
88 form particulate sulfuric acid,¹⁸ and the subsequent neutralization of the sulfuric acid by ambient
89 ammonia to form ammonium sulfate salts^{19,20}:



93 where “g” and “p” denote the gas phase and particle phase, respectively, and “ox” refers to
94 oxidant (in the gas or condensed phase). Since the loadings and composition of the particles are
95 likely to play a role in the human and ecological effects of the plume, it is important that the
96 details and rates of these reactions be well understood. However, while substantial effort has
97 gone into understanding the emissions and chemistry of volcanic SO₂ (as well as trace volcanic

98 species, such as H₂S, HCl, etc.),^{16,17,21-24} the detailed chemistry underlying the formation and
99 evolution of volcano-derived particulate matter has received less study. This is in part due to the
100 challenges associated with measuring particle composition. Mass measurements of PM_{2.5}
101 (particulate matter of diameter 2.5 microns or smaller) are of limited utility for constraining
102 volcanic emissions due to the contribution from non-volcanogenic sources of aerosol, such as
103 fossil fuel burning and dust. Particle composition can be determined from filter-based collection
104 followed by offline chemical analysis,^{3,19,20,24,25} but since sample collection typically requires a
105 few hours to days per filter, such measurements suffer from poor time resolution, providing
106 limited information on temporal variability. Such techniques are also subject to sampling or
107 chemical artifacts, such as from neutralization of acidic sulfate.

108 In this study we apply a relatively new technique, aerosol mass spectrometry,^{26,27} to the
109 characterization of the evolving chemistry of the Kīlauea plume during the first several hours
110 after emission. The high time resolution (a few minutes per measurement) of this technique
111 allows for the characterization of rapid changes in plume chemistry. Volcanic plumes have
112 previously been detected using aerosol mass spectrometry;²⁸⁻³¹ however this represents the first
113 use of the technique in the near-field, aimed at characterizing the temporal variability in particle
114 composition that arises from sulfur oxidation and neutralization reactions. Measurements were
115 made at two different sites, under varying meteorological conditions and plume ages, providing
116 insight into the factors controlling the mass and chemical composition of volcano-derived sulfate
117 particles.

118

119 **Methods.**

120 All measurements were made on the Island of Hawai‘i in January-February 2013, as part of
121 TREX (“Traveling Research Environmental eXperience”), an MIT undergraduate class covering
122 fieldwork in environmental science and engineering. Emissions from the vent of Kīlauea’s
123 Haleama‘uma‘u crater were sampled at two locations over the course of the study (see Figure
124 S1). From January 17 to January 23, measurements were made at Kilauea Military Camp
125 (KMC), located on the north rim of the crater, ~3 km north-northeast of the vent. For these
126 measurements, the instruments were housed inside a minivan, which enabled mobile
127 measurements (not discussed here). Subsequent measurements (January 23 to February 6) were
128 made in the town of Pahala, located 31 km southwest (directly downwind during typical synoptic
129 flow) of the vent. These measurements were taken within the Hawai‘i Department of Health
130 (DOH) air quality monitoring station located in the town.

131 The key chemical measurements were of fine particles (mass concentration and chemical
132 composition) and sulfur dioxide, allowing for the detailed characterization of major sulfur-
133 containing species (sulfate and SO₂) with high (~5 minute) time resolution. Particle mass and
134 composition were measured in real time using an Aerodyne Aerosol Chemical Speciation
135 Monitor (ACSM). The description and operation of this instrument has been described in detail
136 elsewhere.²⁷ Briefly, sampled particles are aerodynamically focused into the high-vacuum
137 detection region, where they are thermally vaporized at 600°C and analyzed using electron
138 impact mass spectrometry. The resulting aerosol mass spectra provide online real-time mass
139 concentrations of non-refractory aerosol species (sulfate, nitrate, ammonium, chloride, and
140 organics). The ACSM detects particles with vacuum aerodynamic diameters of 75-650 nm,
141 which spans nearly the entire accumulation mode, so that all secondary sulfate is likely to be
142 measured. However primary volcanic particles can be somewhat larger than this, with ~50% of

143 the sulfate mass found in particles larger than 650 nm.^{20,25} This might imply that primary sulfate
144 is somewhat underestimated in the present study, though this effect is difficult to quantify, due to
145 the lack of sizing measurements and the unknown role that particulate water plays in controlling
146 particle size. Background sulfate levels (a combination of background ambient levels plus
147 instrumental background) were 0.18 $\mu\text{g}/\text{m}^3$ and 0.075 $\mu\text{g}/\text{m}^3$ at KMC and Pahala, respectively, as
148 determined from measurements during clean periods; these values were subtracted from all
149 measurements to isolate concentrations of volcanic sulfate. At KMC, air was sampled through a
150 1.5 m section of 1/4" OD copper inlet at 1.5 SLPM, positioned out the rear passenger window of
151 the minivan. At Pahala, the PM inlet system was extended (3.7 m total length) in order to co-
152 locate the sampling inlet with that of the DOH instrumentation. A Nafion drier was used to
153 control the relative humidity (30-55%) of the sampled air. Filtered ambient air from a sampling
154 pump (KNF) was used to provide the drier with continuous sheath flow. The temperature and
155 relative humidity of the PM inlet air were monitored and logged throughout the campaign. For
156 all measurements, a collection efficiency of 1 was used, based on the highly acidic nature of the
157 particles.³² Other details of the operation and calibration of the ACSM are given in the
158 Supplementary Information. Measurements were made every 4.8 minutes.

159 SO_2 measurements were made using a UV fluorescence monitor (Teledyne 100E), with
160 ambient air sampled via a 1/4" OD Teflon line co-located with the PM sampling inlet. The
161 instrument was calibrated at the Pahala DOH station with ambient SO_2 , using the measurements
162 from the regularly-calibrated DOH monitor (Thermo Model 43C). Signals from both
163 instruments, spanning several orders of magnitude in SO_2 concentration, were highly correlated
164 ($R^2=0.997$), enabling this in-field calibration. All measurements required a zero-offset correction,
165 which was determined from measurements of air free of volcanic influence, and found to be

166 different at Pahala (1.9 ppb) than at KMC (14.9 ppb). The reason for this difference is not clear,
167 but may be related to the elevation difference (292 vs. 1220 m) at the two sites. SO₂
168 measurements were made every minute, though for comparison with aerosol data they were
169 averaged over the 2.4-minute time periods during which the ACSM was sampling ambient air.

170 Other ancillary measurements include local temperature and relative humidity (Sensirion,
171 1s time resolution), used for calculations of aerosol pH. Wind speed, wind direction, and other
172 meteorological parameters were also measured at the DOH station, though at Pahala these were
173 heavily influenced by local meteorology, namely upslope/downslope flow (Figure S2), and so
174 provide limited insight into the overall trajectory of the volcanic plume. Instead, wind speed and
175 wind direction are taken from the hourly measurements made by the National Park Service
176 (available at <http://ard-request.air-resource.com/>), taken at the USGS Hawaiian Volcano
177 Observatory (HVO). The HVO is located on a flat plain on the northwest rim of the crater, and
178 hence such measurements provide information on the overall meteorology at a given time (e.g.,
179 trade wind conditions vs. stagnant conditions) and thus on the transport of the volcanic plume
180 just after emission.

181

182 **Results and Discussion.**

183 *Meteorological conditions.* Key measurements of the meteorology and sulfur chemistry taken
184 over the course of the entire study (wind speed and direction, [SO₂], and sulfate and ammonium
185 loading) are shown in Figure 1. (All dates and times are local, UTC-10:00.) The meteorological
186 measurements (top panel) indicate that there were five distinct periods during sampling. Two of
187 the periods (period I, Jan. 17-20, and period IV, Jan. 26-30) were characterized by relatively
188 stagnant conditions, with wind speeds below 2 m/s. Two others (II: Jan. 21-23, and V: Jan. 31-

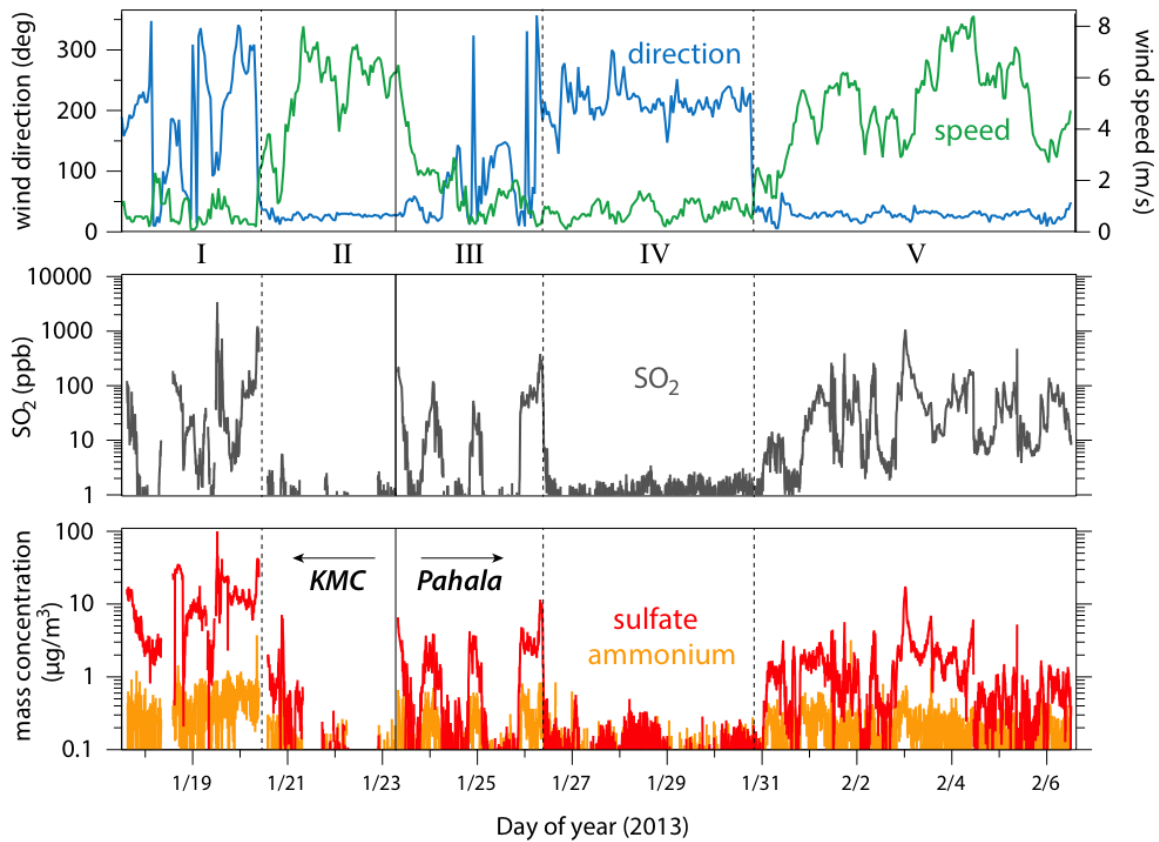


Figure 1. Summary of meteorological parameters and plume composition measurements. Top panel: wind direction (0°/360° refers to wind from due north) and wind speed, measured at HVO near the crater, showing five distinct meteorological conditions during sampling (I and IV: relatively stagnant; II and V: trade winds; III: transitional). Sampling was at KMC (near the crater) during periods I and II and at Pahala (31 km to the southwest) during periods III-V. Middle panel: SO₂ concentrations. Bottom panel: mass concentrations of particulate sulfate and ammonium, as measured by the ACSM.

189 Feb. 6) were characterized by trade winds, with winds coming from the north-northeast at speeds
 190 of 4-8 m/s. Period III (Jan. 23-26) was a transition between trade winds and stagnant conditions,
 191 involving generally weak, northerly winds. The instruments were moved from KMC to Pahala
 192 near the beginning of period III, so both stagnant and trade wind conditions were accessed at
 193 each sampling site. However, the two sites experience very different degrees of volcanic
 194 influence for a given meteorological condition, due to differences in the positions of the two sites
 195 relative to the vent. During stagnant periods, volcanic emissions affect KMC but not Pahala,
 196 whereas trade winds send the emissions directly towards Pahala, leaving the air at KMC

197 essentially free of direct volcanic influence. Thus the periods in which volcanic influence is
198 expected to be observed are period I (stagnant air, sampling at KMC) and period V (trade winds,
199 sampling at Pahala), and to a lesser extent period III (weak northerly winds, sampling at Pahala).
200 Measured SO₂ and sulfate levels (bottom two panels) are indeed highest during these periods,
201 indicating that this simple description of the meteorology provides insight into the fate and
202 transport of the volcanic plume.

203

204 *SO₂, sulfate, and sulfur partitioning.* Measured SO₂ levels (Fig. 1, middle panel) varied over an
205 extremely wide range, from below 1 ppb (for times with no volcanic influence, periods II and
206 IV) to over 3 ppm (stagnant conditions at KMC). Exceedingly high levels (>1 ppm) are also
207 measured during times of trade wind influence in Pahala. Such high concentrations more than 30
208 km downwind of the source indicate the sustained intensity of the volcanic plume even after
209 substantial advection. These high SO₂ levels are not unusual for Pahala, since trade wind
210 conditions persist throughout the year, especially in non-winter months (see Figure S3).

211 Particulate sulfate levels (Fig. 1, bottom panel) were also high (up to ~100 µg/m³) during
212 periods of volcanic influence. Ammonium levels were generally measureable but small (usually
213 <1 µg/m³), indicating relatively little neutralization of the sulfate aerosol. The role of
214 neutralization and aerosol acidity will be discussed below. Other particulate species measured by
215 the ACSM (not shown) were minor; the one exception is organic aerosol, which occasionally
216 spiked at KMC due to local wood burning emissions, but this had no apparent influence on
217 sulfate measurements. Measured chloride levels were negligible, consistent with recent work
218 finding low Cl emissions from Kīlauea relative to other volcanoes.²⁴

219 While SO₂ and sulfate tend to co-vary (i.e., both are high during periods of volcanic
220 influence), the overall correlation between the two species is relatively poor ($R^2=0.37$; see Figure
221 S4), indicating large variability in the extent of sulfur fractionation over the course of the study.
222 Figure 2 shows how the partitioning of sulfur between the two species varied over the course of
223 the study. Partitioning is expressed in terms of the fraction f_s of total sulfur in the form of
224 particulate sulfate, given by $f_s=[SO_4^{2-}]/([SO_4^{2-}]+[SO_2])$, with all concentrations in molar units.³³
225 This calculation assumes that all sulfate is measured by the ACSM; if some fraction is not (e.g.,
226 some of the sulfate is present in particles outside the ACSM's size window), then the derived f_s
227 value will be somewhat of an underestimate. For periods in which volcanic influence was
228 minimal (II and IV), partitioning is likely controlled by non-volcanogenic sources of sulfur, and
229 is subject to considerable uncertainty, given the low concentrations of both species. The volcano-
230 influenced periods (I, III, V) exhibit substantial variability in sulfur partitioning. While
231 differences in relative deposition rates may contribute to this variability, the main source is likely
232 differences in photochemical age, the extent of oxidative processing between emission and
233 measurement. Under low-wind conditions, the SO₂ emissions can accumulate and over time
234 convert to sulfate, leading to the large values of f_s in periods I and III. By contrast, under trade
235 wind conditions (period V), the volcanic plume intercepted at Pahala was no more than a few
236 hours old, with little time for SO₂-to-sulfate conversion, leading to much lower values of f_s . The
237 relatively high value of f_s on Jan. 31 may have resulted from the onset of the trade winds,
238 leading to advection of relatively aged emissions from the crater to Pahala.

239

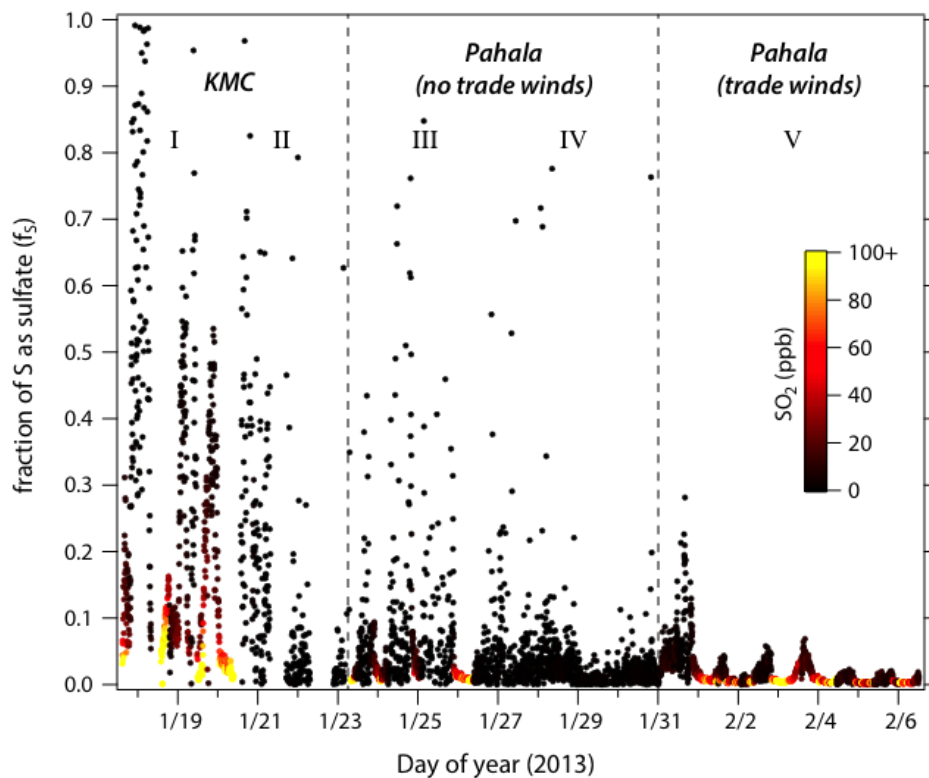


Figure 2. Measured sulfur partitioning (f_s) over the course of the study. Points are colored by SO_2 concentration. For times influenced by volcanic emissions, it is highest when the winds are lowest (periods I and III). During trade wind conditions, there is a clear diurnal pattern in f_s downwind of the crater (period V).

240
 241 SO_2 oxidation kinetics. Period V (trade wind conditions, sampling at Pahala) is characterized by
 242 a clear diurnal cycle in sulfur partitioning, with f_s lowest at night and highest in the afternoon.
 243 Dry deposition might lead to changes in f_s , due to differences in deposition rates of SO_2 and
 244 sulfate.³⁴ However such differences are highly unlikely to exhibit the observed diurnal profile in
 245 f_s , which changes by up to a factor of 8 over the course of the day. Instead, this time-of-day
 246 dependence strongly suggests that the SO_2 -to-sulfate conversion is driven by photochemical
 247 oxidation. Such oxidation is likely due to reaction with short-lived oxidants. Oxidation catalyzed
 248 by transition metal ions³⁵ is unlikely to be important, given that oxidation is primarily observed
 249 during the daytime only. Similarly, oxidation by aqueous O_3 is expected to be negligible, due to

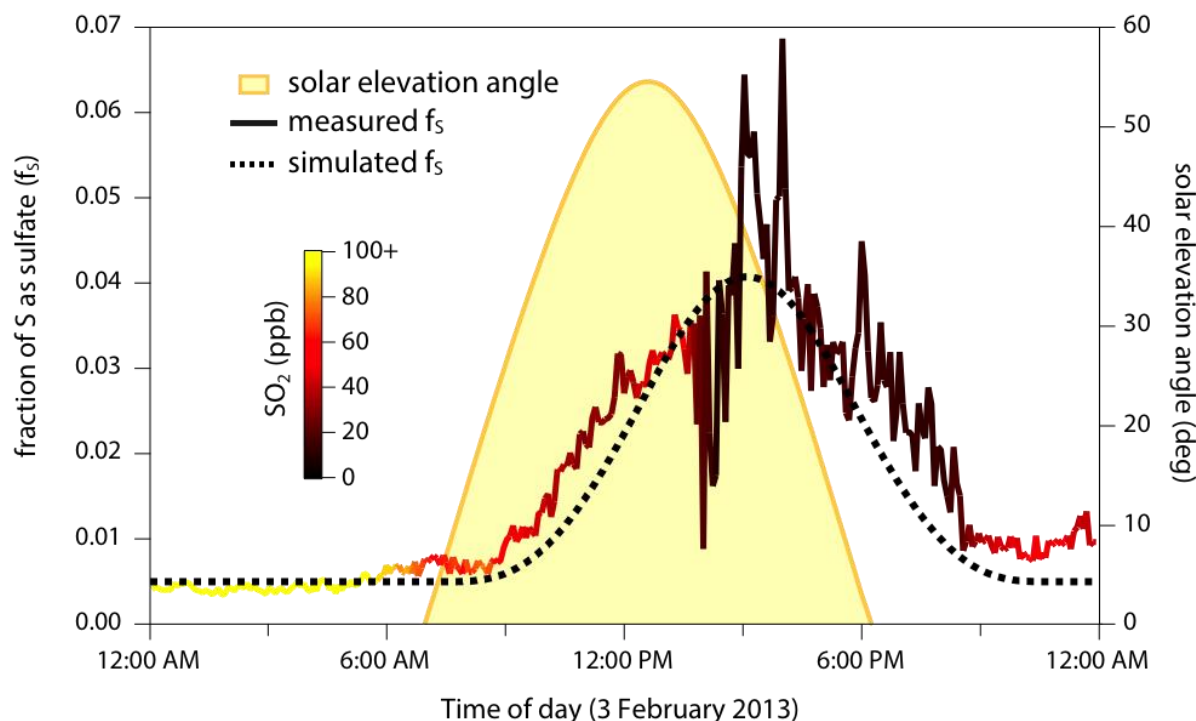


Figure 3. Evolving sulfur partitioning (f_s) at Pahala on Feb. 3, 2013 (a day characterized by trade winds). The diurnal profile in f_s (thick trace) indicates sunlight-initiated SO_2 oxidation to sulfate. Partitioning lags behind solar elevation angle (a metric of irradiation, shown in yellow), due to the transport time from the source to the sampling site. The dashed line denotes calculated f_s from a simple kinetic model matched to the observations; this enables estimates of the primary sulfate fraction (0.005), age of the plume (~ 5 hours), and instantaneous SO_2 oxidation rate ($2.4 \times 10^6 \text{ s}^{-1}$ at solar noon).

250 the high acidity of the particles. Oxidation by Criegee intermediates³⁶ is also unlikely given the
 251 presumably low concentrations of VOCs in the plume. Thus the dominant oxidants are likely to
 252 be photolytically-generated species, such as gas-phase OH or aqueous H_2O_2 .

253 The evolving sulfur partitioning for a single day (Feb. 3) is shown in greater detail in
 254 Figure 3, along with that day's solar elevation angle (SEA). Before sunrise, both SO_2 and sulfate
 255 are at their highest levels of the day (likely due in part to the shallow boundary layer), but the
 256 sulfate fraction is at a minimum. At sunrise, the sulfate fraction starts increasing, reaching a peak
 257 of several percent in the afternoon before falling back to almost the previous night's value. This
 258 time dependence is similar during other days in period V, though with lower peak values of f_s
 259 (Fig. 2).

260 Figure 3 shows a considerable lag between solar irradiation (which peaks at solar noon,
261 12:35pm) and the peak in measured fractional sulfur conversion (which peaks at ~3:00pm);
262 elevated sulfate fractions are observed well after sunset. This time lag arises at least in part from
263 the time elapsed between emission and sampling, since the conversion of SO₂ to sulfate is
264 governed by exposure to oxidants, which varies dramatically over the course of the day.

265 In order to better quantify this oxidation process, a simple kinetic model was constructed
266 to relate transit time, SO₂ oxidation rate, and fractional sulfur conversion. First, some fraction of
267 the sulfur is assumed to be primary (directly emitted from the volcano). This fraction, taken from
268 the zero-offset in Fig. 3, is ~0.005, consistent with previous measurements of primary sulfate
269 emissions (on the order of 0.1-1% of total sulfur^{3,20,37,38}); however errors in the present value
270 may arise from the size cutoff of the ACSM, and/or the potential contribution of secondary
271 production of sulfate via nighttime oxidation of SO₂. Oxidation (the increase in f_s) is then
272 simulated by assuming that the instantaneous oxidation rate is proportional to the ozone
273 photolysis rate constant J(O¹D) (i.e., that oxidation is driven by OH, or another oxidant with a
274 similar diurnal profile). The time-of-day dependence of J(O¹D) is estimated from SEA using the
275 parameterization used in the Master Chemical Mechanism;³⁹ cloud cover was minimal on this
276 day. Since oxidation occurs continually over the time between emission and sampling, the model
277 integrates J(O¹D) over some fixed transit time; this time is determined by adjusting it to match
278 the peak in f_s. We note that if the observed time lag derives not only from the transport time but
279 also from oxidant levels peaking later in the day (which would require the oxidants to be
280 substantially longer-lived than OH), the transport time estimated using this approach would
281 represent an upper limit. Finally, the instantaneous (time-dependent) SO₂ oxidation rate (s⁻¹) is
282 determined from this transit time, by adjusting the proportionality constant that relates J(O¹D) to

283 oxidation rate until the integrated amount of oxidation matches the observed f_s values (height of
284 the paraboloid in Fig. 3). Dry deposition is not explicitly included in the model; it is a highly
285 uncertain process which, as discussed above, might affect f_s but likely not with the diurnal
286 dependence observed.

287 Model results are shown as the dashed line in Fig. 3; with the exception of the slightly
288 narrower peak in simulated f_s (discussed below), the model reproduces the time-dependent f_s
289 measurements well. Interestingly, the peak in the observed sulfate fraction can be reproduced
290 only by assuming a five-hour transit time, substantially longer than what would be expected
291 based on wind speed and distance alone (~1.5 hours). As noted above, this inferred transit time
292 may be somewhat of an overestimate if sulfate formation is driven by long-lived oxidants that
293 peak late in the day. Nonetheless this result suggests that the plume was not transported directly
294 to Pahala but rather was influenced by local topographic and meteorological factors, a conclusion
295 that is strongly supported by measured differences in local winds at the crater and Pahala (Fig.
296 S2). During these trade wind days (period V, 1/31/13-2/7/13), winds at the crater were mostly
297 from the north-northeast, with an average speed of 6.8 m/s, whereas at Pahala the winds were
298 predominantly from the east/southeast (in the morning) or northwest (in the afternoon and night),
299 with an average speed of only 2.0 m/s. Thus, even on trade wind days the volcanic plume did
300 not take a direct path from the crater to Pahala, but rather reached Pahala via upslope/downslope
301 flow. This longer transit distance and slower wind speed implies a substantially longer transit
302 time than would be expected based on the simple (and commonly-used) calculation based on
303 wind speed and distance, in agreement with our observations. Fig. S2 also indicates that the
304 transit time likely varies over the course of the day; this may explain why our simple model does

305 not fully capture the observed time-dependence of the oxidation (somewhat underestimating the
306 width of the paraboloid in Fig 3).

307 The model also provides an estimate of the time-dependent SO₂ oxidation rate. The
308 maximum (noontime) oxidation rate is $2.4 \times 10^{-6} \text{ s}^{-1}$, and the 24-hour average oxidation rate is
309 $5.3 \times 10^{-7} \text{ s}^{-1}$, yielding an SO₂ lifetime vs. oxidation under these conditions of ~22 days. To our
310 knowledge this represents the first diurnally-resolved measurement of the instantaneous SO₂
311 oxidation rate within a volcanic plume. Assuming the oxidation is by gas-phase OH (and using
312 $k_{\text{OH}+\text{SO}_2} = 8.9 \times 10^{-13} \text{ cm}^3 \text{ molec}^{-1} \text{ s}^{-1}$)⁴⁰, these observed rates correspond to an equivalent peak
313 [OH] of $2.7 \times 10^6 \text{ molec cm}^{-3}$, and an equivalent diurnally-averaged [OH] of $5.9 \times 10^5 \text{ molec cm}^{-3}$.
314 Such concentrations are lower than typical ambient values of [OH] for the tropics,⁴¹ suggesting
315 suppression of OH within the plume, presumably due to the very high SO₂ concentrations.

316 The measured rate of SO₂ oxidation ($5.3 \times 10^{-7} \text{ s}^{-1}$) is on the low end of previous estimates
317 of SO₂ loss rates within tropospheric volcanic plumes, which range from $2 \times 10^{-7} \text{ s}^{-1}$ to $\sim 10^{-4}$
318 s^{-1} .^{8,18,20,25,28,33,42-48} (Some near-field measurements⁴⁹ found even faster rates of loss ($> 10^{-3} \text{ s}^{-1}$),
319 though those measurements may have been biased high due to variations in emissions.¹⁸) In fact,
320 on subsequent trade wind days (Feb. 4-6) the estimated oxidation rate is lower still (by a factor of
321 2-3), making our measurements of SO₂ oxidation rate among the lowest ever reported. Focusing
322 on Kīlauea only, two previous studies (one ground-based⁴⁵ and one satellite-based⁸) of SO₂ from
323 Kīlauea found the conversion time to be $5.8 \times 10^{-6} - 1.2 \times 10^{-5} \text{ s}^{-1}$ and $3.2 \times 10^{-5} \text{ s}^{-1}$, respectively, both
324 significantly faster than the rate determined here. Even if the transit time is shorter than the
325 inferred value of five hours, and instead is closer to the lower-limit value of 1.5 hours (which, as
326 discussed above, is likely an underestimate), the inferred oxidation rates would increase by only
327 a factor of 3.3, and thus are still lower than most previous measurements.

328 Part of the reason for the differences between determined rates may be methodological.
329 In the present study, both SO₂ and sulfate are measured directly, and primary sulfate is explicitly
330 accounted for; in studies in which sulfate is not directly measured but rather inferred, calculated
331 rates can be influenced (mostly overestimated) by losses of SO₂ via non-oxidative processes
332 (dilution, deposition), the presence of non-sulfate components of aerosol (e.g., water, ash,
333 ammonium), and the importance of primary volcanic sulfate. In addition, since the present
334 approach is based on fractional sulfur conversion, it does not assume that SO₂ emissions are
335 fixed, as assumption that can also complicate determinations of conversion rates.¹⁸ Most
336 importantly, the use of solar irradiation for determining the age of the sampled emissions is a
337 unique feature of the present analysis. Most previous studies instead estimate age from average
338 wind speed and distance; in areas with complex terrain and local meteorology, such as that of the
339 present study, this approach can underestimate plume age, which would also lead to an
340 overestimate in oxidation rate.

341 Despite the above considerations, the differences in inferred reactivities in the present
342 study and in previous work may reflect real differences in plume composition and ambient
343 oxidative conditions, leading to substantial variability in SO₂ oxidation rate. Our measurements
344 were made in the wintertime, which (even in the tropics) is characterized by lower
345 photochemical activity than in summer months;⁴¹ the previous measurements of SO₂ oxidation
346 within the Kīlauea plume were made in August⁴⁵ and March-November,⁸ which may help
347 explain the higher rates inferred in those studies. In addition, the plumes sampled in the present
348 work were very well-defined, with sustained high SO₂ concentrations that would drive down
349 oxidant levels. By contrast, less-concentrated plumes may be significantly more photochemically

350 active, leading to SO₂ oxidation rates that would be substantially higher than the ones determined
351 here.

352 For the earlier, non-trade-wind periods, the above approach for estimating plume age and
353 SO₂ oxidation rate cannot be applied, due to the lack of rapid, stable transport of emissions from
354 the vent to the sampling site. The air sampled was therefore made up of emissions that span a
355 wide range of atmospheric ages; such a system is not easily analyzed using simple kinetics,
356 especially given the lack of measurements that could help constrain the time of emission.
357 Instead, we use [SO₂] as a qualitative metric for the average plume age, since it provides
358 information about the amount of dispersion that has taken place since emission (assuming
359 emissions remain roughly constant).

360 Shown in Figure 4 are plots of f_s vs. [SO₂] for times of major volcanic influence (periods
361 I and V). Only data with [SO₂] ≥ 10 ppb are shown, in order to avoid errors associated with
362 background concentrations and instrument zeroes. The coloring within the different panels is
363 related to particle acidity, described below. The sulfur in fresh volcanic emissions is highly
364 concentrated and present mostly in the form of [SO₂]. The average value of f_s for these fresh
365 emissions (lower right corner of Fig. 4), which corresponds to the fraction of sulfur emitted as
366 primary volcanic sulfate, is ~0.008. This is slightly higher than the value inferred downwind
367 (Fig. 3), though again this may be an underestimate given the size cutoff of the ACSM.
368 Dispersion of the emissions (dilution) leads to leftward movement in Fig. 4, since SO₂ and
369 sulfate are affected essentially equally. (Some changes to f_s may occur in the most dilute cases,
370 due to the entrainment of background air.) Oxidation leads to an increase in f_s , for upward (and
371 slightly leftward) movement. A third process, deposition, also involves movement towards lower
372 [SO₂] and slightly higher f_s , due to differences in SO₂ and sulfate deposition velocities.³⁴

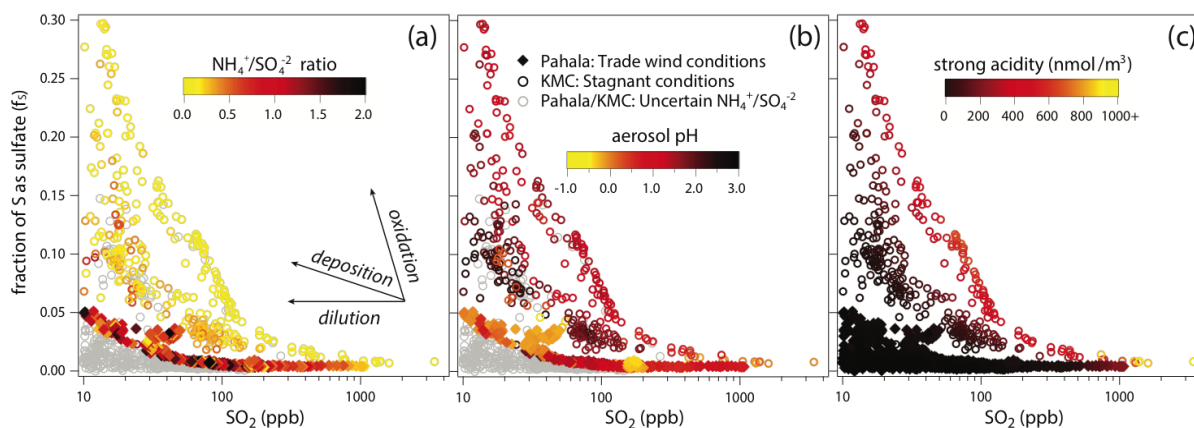


Figure 4. Changes to volcanic emissions due to dilution, deposition, oxidation, and neutralization. Measurements from periods I (KMC, stagnant) and V (Pahala, trade winds) are shown, plotted as f_s (sulfur partitioning) vs. $[SO_2]$ (a rough measure of plume dispersion since emission). Movement in this space corresponds to different processes affecting sulfate levels (dilution, deposition, and oxidation), as shown by the arrows in panel a. Marker color denotes degree of neutralization, with yellow denoting the most acidic particles, using three different acidity metrics. Panel a: ammonium/sulfate ratio. Panel b: aerosol pH. Panel c: strong acidity.

373 The extent of sulfate conversion is generally much greater at KMC than at Pahala. This
374 indicates substantially more SO_2 oxidation under stagnant conditions, due to differences in
375 plume age and/or oxidation rate. The Pahala plume was intercepted only ~ 5 hours after
376 emissions, whereas the emissions sampled at KMC could have been up to several days old, since
377 the stagnation event had begun a week earlier (on Jan. 12). However, age of the emissions cannot
378 fully explain the differences in f_s in the two cases, since SO_2 reactivity also appears to vary.
379 Even assuming an average age of 3 days (which is likely an upper limit), the f_s value of 0.3
380 would correspond to an average SO_2 oxidation rate of $1.4 \times 10^{-6} \text{ s}^{-1}$, which is more than twice as
381 fast as the rate on Feb. 3. Differences in oxidation rate in the two cases are even more
382 pronounced if it is assumed that measured emissions are younger than this, and/or when these
383 inferred rates are compared against those from the other trade wind days (Feb. 4-6). This
384 increased SO_2 reactivity at KMC suggests the presence of higher oxidant levels (in either the gas
385 or droplet phase) in this stagnant case.

386

387 *Particle acidity and neutralization.* The sulfur-partitioning data in Fig. 4 are colored according to
388 particle acidity, with the color scale in each panel corresponding to a different acidity metric.
389 Figure 4a shows the ammonium-to-sulfate ($[\text{NH}_4^+]/[\text{SO}_4^{2-}]$) ratio, as measured by the ACSM.
390 Only ratios for which the absolute uncertainty is below 0.5 are shown; uncertainties were
391 calculated from the scatter in the measurement of each aerosol component (1σ : $0.09 \mu\text{g}/\text{m}^3$ for
392 $[\text{NH}_4^+]$ and $0.08 \mu\text{g}/\text{m}^3$ for $[\text{SO}_4^{2-}]$, based on clean-air measurements). The aerosol is only
393 slightly neutralized by ammonia, with ratios mostly ranging from 0 (pure sulfuric acid) to 1
394 (ammonium bisulfate). While aerosol mass spectrometry (AMS) measurements have previously
395 found sulfate particles of volcanic origin to be acidic,²⁹⁻³¹ to our knowledge these measurements
396 constitute the first AMS measurement of pure sulfuric acid particles in the ambient atmosphere.
397 Levels of neutralization of the sulfate at Pahala are higher than at KMC, presumably due to
398 terrestrial ammonia emissions encountered by the plume as it travels downwind over land, which
399 includes agricultural areas. This is consistent with previous studies that also found increased
400 ammonium levels in particles downwind of volcanic emissions.^{19,20}

401 Data in Fig. 4b are colored by aerosol pH (a measure of acidity within the particles),
402 calculated using the Extended Aerosol Inorganics Model (E-AIM, Model II:
403 <http://www.aim.env.uea.ac.uk/aim/aim.ph>)⁵⁰, and assuming the only counterions are H^+ or NH_4^+ .
404 Inputs to the model are sulfate, ammonium, ambient relative humidity, and ambient temperature,
405 and pH is determined from the calculated activity coefficients and concentrations of $[\text{H}^+]$. As in
406 Fig. 4a, only the pH values for data whose $[\text{NH}_4^+]/[\text{SO}_4^{2-}]$ ratios can be determined to within 0.5
407 are shown. The particles are highly acidic, ranging in pH from -0.8 (the equivalent of 6M H_2SO_4)
408 to 3.0. At such high acidity, the pH values actually do not correlate strongly with $[\text{NH}_4^+]/[\text{SO}_4^{2-}]$,

409 since this ratio does not vary over a wide range. Instead pH is mostly a function of ambient RH,
410 with drier conditions (such as those encountered at Pahala) leading to less water uptake by the
411 sulfate, and thus higher H^+ activities within the particles.

412 Finally, the points in Fig. 4c are colored by strong acidity (a measure of acidity per
413 volume of air), determined from $2 \times [SO_4^{2-}] - [NH_4^+]$. Unlike the other two metrics of acidity
414 ($[NH_4^+]/[SO_4^{2-}]$ and pH), strong acidity can be precisely determined even when $[NH_4^+]$ and
415 $[SO_4^{2-}]$ are low, so values for all measurements are shown. Given the low level of neutralization
416 of the particles, strong acidity depends largely on absolute sulfate levels, and so is poorly
417 correlated with particle pH (which depends mostly on RH); thus acidity normalized to the
418 volume of air and acidity normalized to the volume of the particles are largely independent
419 quantities in this case. Sulfate levels are highest during the stagnant days at KMC, leading to
420 extremely high strong acidity values, of hundreds of $nmol/m^3$ when sampling aged emissions,
421 and up to $2200 nmol/m^3$ when sampling fresh emissions. These values are far higher than those
422 typically measured in ambient air, even under polluted urban conditions (where typical values
423 are in the range of $50-200 nmol/m^3$).^{51,52}

424
425 *Implications and future work.* In general, measuring the chemistry and effects of individual
426 emissions sources can be challenging, due to complex and variable meteorology, uncertain
427 chemical reactions, and interferences from other sources (background levels) of pollutants.
428 However the Kīlauea plume is in many ways an ideal system for measuring evolving plume
429 chemistry: the prevailing meteorology is simple (enabling estimates of plume age), the key
430 chemical transformations are relatively well-understood, and the point source is very intense and
431 emits into clean air. These conditions, when coupled with highly time-resolved measurements of

432 particle mass and chemical composition (as well as concentrations of the gas-phase precursor),
433 allow for the detailed characterization of the factors controlling the formation and evolution of
434 secondary particulate matter.

435 The real-time measurements made in this study show that the volcanic plume is highly
436 variable and dynamic, and depends not only on emission rate and meteorology, but also on other
437 factors that can vary strongly with location, time of day, and time of year. These include the
438 daytime oxidant production (controlling SO₂ oxidation rate), as well as local emissions and
439 relative humidity (controlling particle acidity). The effects of volcanic emissions on human and
440 ecological health may thus also exhibit dependences on these factors; this is an important area of
441 future research. Also important is the extension of these measurements to a wider range of
442 locations and plume ages. In particular, time-resolved composition measurements at locations
443 still further downwind will provide information on the role of plume chemistry over longer
444 timescales, as well as on the exposure to downwind communities to various components of the
445 volcanic plume.

446

447 **Acknowledgments.**

448 Funding for this project was provided by MIT's Department of Civil and Environmental
449 Engineering. We are grateful to the Hawai'i State Department of Health for access to their air
450 quality monitoring station (Pahala measurements) and data; and to the National Park Service for
451 permitting research within Hawai'i Volcanoes National Park (KMC measurements, research
452 permit HAVO-2012-SCI-0047) and for their online meteorological data. We also thank MIT's
453 Sloan Engine Laboratory for use of their SO₂ monitor; Tamar Elias, Andrew J. Sutton, and Paul

454 G. Okubo of the USGS Hawaiian Volcano Observatory for helpful advice, suggestions, and
455 support; and Denise Miller for invaluable assistance with lodging and logistics.

456

457

458 **Supporting Information Available.**

459 Details of the ACSM operation and calibration, plus Figures S1-S4, showing: (S1) a map of the
460 Island of Hawai‘i, with locations of volcanic vents and sampling sites; (S2) wind speed and
461 direction at HVO and Pahala, showing differences in local meteorology at the two sites, (S3)
462 cumulative probability distributions of SO₂ concentrations at Pahala, and (S4) a plot of sulfate
463 mass concentration vs. SO₂ concentration for all measurements. This information is available
464 free of charge via the Internet at <http://pubs.acs.org/>.

465

466 **References.**

- 467 (1) Schmidt, A.; Carslaw, K. S.; Mann, G. W.; Rap, A.; Pringle, K. J.; Spracklen, D. V.; Wilson,
468 M.; Forster, P. M. Importance of tropospheric volcanic aerosol for indirect radiative forcing
469 of climate. *Atmos. Chem. Phys.* **2012**, *12*, 7321–7339.
- 470 (2) Andres, R. J.; Kasgnoc, A. D. A time- averaged inventory of subaerial volcanic sulfur
471 emissions. *J. Geophys. Res. Atmos.* **1998**, *103*, 25251–25261.
- 472 (3) Allen, A. G.; Oppenheimer, C.; Ferm, M.; Baxter, P. J.; Horrocks, L. A.; Galle, B.;
473 McGonigle, A. J. S.; Duffell, H. J. Primary sulfate aerosol and associated emissions from
474 Masaya Volcano, Nicaragua. *J. Geophys. Res.* **2002**, *107*, ACH5-1–ACH5-8.
- 475 (4) IPCC. Climate Change 2013: The Physical Science Basis; Stocker, T. F.; Qin, D.; Plattner,
476 G.-K.; Tignor, M. M. B.; Allen, S. K.; Boschung, J.; Nauels, A.; Xia, Y.; Bex, V.; Midgely,
477 P. M., Eds.; Cambridge University Press: Cambridge, UK, 2013; p. 1535.
- 478 (5) Small, C.; Naumann, T. The global distribution of human population and recent volcanism.
479 *Environmental Hazards* **2001**, *3*, 93–109.
- 480 (6) Hansell, A.; Oppenheimer, C. Health hazards from volcanic gases: a systematic literature
481 review. *Arch. Environ. Health* **2004**, *59*, 628–639.
- 482 (7) Hansell, A. L. The health hazards of volcanoes and geothermal areas. *Occupational and*
483 *Environmental Medicine* **2006**, *63*, 149–156.
- 484 (8) Beirle, S.; Hörmann, C.; Penning de Vries, M.; Dörner, S.; Kern, C.; Wagner, T. Estimating
485 the volcanic emission rate and atmospheric lifetime of SO₂ from space: a case study for
486 Kīlauea volcano, Hawai`i. *Atmos. Chem. Phys.* **2014**, *14*, 8309–8322.
- 487 (9) EPA. The 2011 National Emissions Inventory; 1st ed.; 2012.
- 488 (10) Mannino, D. M.; Ruben, S. M.; Holschuh, F. C.; Holschuh, T. C.; Wilson, M. D.;
489 Holschuh, T. Emergency department visits and hospitalizations for respiratory disease on the
490 Island of Hawaii, 1981-1991. *Hawaii Medical Journal* **1996**, *55*, 48–54.
- 491 (11) Longo, B. M.; Rossignol, A.; Green, J. B. Cardiorespiratory health effects associated with
492 sulphurous volcanic air pollution. *Public Health* **2008**, *122*, 809–820.
- 493 (12) Longo, B. M.; Yang, W. Acute Bronchitis and Volcanic Air Pollution: A Community-
494 Based Cohort Study at Kilauea Volcano, Hawai`i, USA. *Journal of Toxicology and*
495 *Environmental Health, Part A* **2008**, *71*, 1565–1571.
- 496 (13) Longo, B. M. The Kilauea Volcano adult health study. *Nursing research* **2009**, *58*, 23–
497 31.
- 498 (14) Longo, B. M.; Yang, W.; Green, J. B.; Crosby, F. L.; Crosby, V. L. Acute Health Effects
499 Associated with Exposure to Volcanic Air Pollution (vog) from Increased Activity at Kilauea
500 Volcano in 2008. *Journal of Toxicology and Environmental Health, Part A* **2010**, *73*, 1370–
501 1381.
- 502 (15) Longo, B. M. Adverse Health Effects Associated with Increased Activity at Kīlauea
503 Volcano: A Repeated Population-Based Survey. *ISRN Public Health* **2013**, *2013*, 1–10.
- 504 (16) von Glasow, R. Atmospheric chemistry in volcanic plumes. *Proc. Natl. Acad. Sci. U.S.A.*
505 **2010**, *107*, 6594–6599.

- 506 (17) von Glasow, R.; Bobrowski, N.; Kern, C. The effects of volcanic eruptions on
507 atmospheric chemistry. *Chemical Geology* **2009**, *263*, 131–142.
- 508 (18) McGonigle, A.; Delmelle, P.; Oppenheimer, C.; Tsanev, V. I.; Delfosse, T.; Williams
509 Jones, G.; Horton, K.; Mather, T. A. SO₂ depletion in tropospheric volcanic plumes.
510 *Geophys. Res. Lett.* **2004**, *31*.
- 511 (19) Allen, A. G.; Baxter, P. J.; Ottley, C. J. Gas and particle emissions from Soufrière Hills
512 Volcano, Montserrat, West Indies: characterization and health hazard assessment. *Bulletin of*
513 *Volcanology* **2000**, *62*, 8–19.
- 514 (20) Mather, T. A.; Allen, A. G.; Oppenheimer, C.; Pyle, D. M.; McGonigle, A. J. S. Size-
515 Resolved Characterisation of Soluble Ions in the Particles in the Tropospheric Plume of
516 Masaya Volcano, Nicaragua: Origins and Plume Processing. *J Atmos Chem* **2003**, *46*, 207–
517 237.
- 518 (21) Oppenheimer, C.; Scaillet, B.; Martin, R. S. Sulfur Degassing From Volcanoes: Source
519 Conditions, Surveillance, Plume Chemistry and Earth System Impacts. *Reviews in*
520 *Mineralogy and Geochemistry* **2011**, *73*, 363–421.
- 521 (22) Mather, T. A. Volcanism and the atmosphere: the potential role of the atmosphere in
522 unlocking the reactivity of volcanic emissions. *Philosophical Transactions of the Royal*
523 *Society A: Mathematical, Physical and Engineering Sciences* **2008**, *366*, 4581–4595.
- 524 (23) Edmonds, M.; Sides, I. R.; Swanson, D. A.; Werner, C.; Martin, R. S.; Mather, T. A.;
525 Herd, R. A.; Jones, R. L.; Mead, M. I.; Sawyer, G.; Roberts, T. J.; Sutton, A. J.; and Elias, T.
526 Magma storage, transport and degassing during the 2008–10 summit eruption at Kīlauea
527 Volcano, Hawai‘i. *Geochimica et Cosmochimica Acta* **2013**, *123*, 284–301.
- 528 (24) Mather, T. A.; Witt, M. L. I.; Pyle, D. M.; Quayle, B. M.; Aiuppa, A.; Bagnato, E.;
529 Martin, R. S.; Sims, K. W. W.; Edmonds, M.; Sutton, A. J.; Ilyinskaya, E. Halogens and trace
530 metal emissions from the ongoing 2008 summit eruption of Kīlauea volcano, Hawai‘i.
531 *Geochimica et Cosmochimica Acta* **2012**, *83*, 292–323.
- 532 (25) Mather, T. A.; Tsanev, V. I.; Pyle, D. M.; McGonigle, A. J. S.; Oppenheimer, C.; Allen,
533 A. G. Characterization and evolution of tropospheric plumes from Lascar and Villarrica
534 volcanoes, Chile. *J. Geophys. Res.* **2004**, *109*, D21303.
- 535 (26) Canagaratna, M. R.; Jayne, J. T.; Jimenez, J. L.; Allan, J. D.; Alfarra, M. R.; Zhang, Q.;
536 Onasch, T. B.; Drewnick, F.; Coe, H.; Middlebrook, A.; Delia, A.; Williams, L. R.;
537 Trimborn, A. M.; Northway, M. J.; DeCarlo, P. F.; Kolb, C. E.; Davidovits, P.; Worsnop, D.
538 R. Chemical and microphysical characterization of ambient aerosols with the aerodyne
539 aerosol mass spectrometer. *Mass Spectrom. Rev.* **2007**, *26*, 185–222.
- 540 (27) Ng, N. L.; Herndon, S. C.; Trimborn, A.; Canagaratna, M. R.; Croteau, P. L.; Onasch, T.
541 B.; Sueper, D.; Worsnop, D. R.; Zhang, Q.; Sun, Y. L.; Jayne, J. T. An Aerosol Chemical
542 Speciation Monitor (ACSM) for Routine Monitoring of the Composition and Mass
543 Concentrations of Ambient Aerosol. *Aerosol Science and Technology* **2011**, *45*, 780–794.
- 544 (28) Carn, S. A.; Froyd, K. D.; Anderson, B. E.; Wennberg, P.; Crounse, J.; Spencer, K.;
545 Dibb, J. E.; Krotkov, N. A.; Browell, E. V.; Hair, J. W.; Diskin, G.; Sachse, G.; Vay, S. A. In
546 situ measurements of tropospheric volcanic plumes in Ecuador and Colombia during TC⁴. *J.*
547 *Geophys. Res.* **2011**, *116*, D00J24.

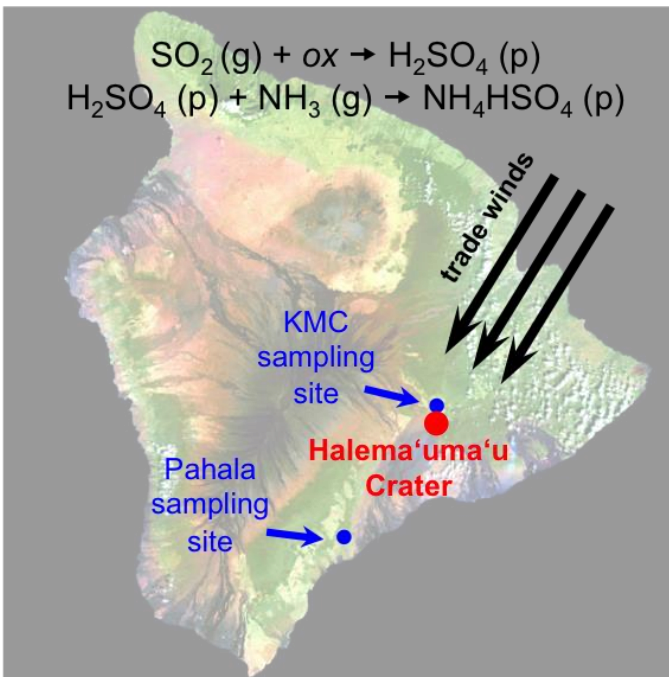
- 548 (29) DeCarlo, P. F.; Dunlea, E. J.; Kimmel, J. R.; Aiken, A. C.; Sueper, D.; Crounse, J.;
549 Wennberg, P. O.; Emmons, L.; Shinozuka, Y.; Clarke, A. Fast airborne aerosol size and
550 chemistry measurements above Mexico City and Central Mexico during the MILAGRO
551 campaign. *Atmos. Chem. Phys.* **2008**, *8*, 4027–4048.
- 552 (30) Ovadnevaite, J.; Ceburnis, D.; Plauskaite-Sukiene, K.; Modini, R.; Dupuy, R.; Rimselyte,
553 I.; Ramonet, M.; Kvietkus, K.; Ristovski, Z.; Berresheim, H.; O'Dowd, C. D. Volcanic
554 sulphate and arctic dust plumes over the North Atlantic Ocean. *Atmospheric Environment*
555 **2009**, *43*, 4968–4974.
- 556 (31) O'Dowd, C.; Ceburnis, D.; Ovadnevaite, J.; Martucci, G.; Bialek, J.; Monahan, C.;
557 Berresheim, H.; Vaishya, A.; Grigas, T.; Jennings, S. G.; McVeigh, P.; Varghese, S.;
558 Flanagan, R.; Martin, D.; Moran, E.; Lambkin, K.; Semmier, T.; Perrino, C.; McGrath, R.
559 The Eyjafjallajökull ash plume - Part I: Physical, chemical and optical characteristics.
560 *Atmospheric Environment* **2012**, *48*, 129–142.
- 561 (32) Matthew, B. M.; Middlebrook, A. M.; Onasch, T. B. Collection Efficiencies in an
562 Aerodyne Aerosol Mass Spectrometer as a Function of Particle Phase for Laboratory
563 Generated Aerosols. *Aerosol Science and Technology* **2008**, *42*, 884–898.
- 564 (33) Satsumabayashi, H.; Kawamura, M.; Katsuno, T.; Futaki, K.; Murano, K.; Carmichael,
565 G. R.; Kajino, M.; Horiguchi, M.; Ueda, H. Effects of Miyake volcanic effluents on airborne
566 particles and precipitation in central Japan. *J. Geophys. Res.* **2004**, *109*.
- 567 (34) Walcek, C. J.; Brost, R. A.; Chang, J. S.; Wesely, M. L. SO₂, sulfate and HNO₃
568 deposition velocities computed using regional landuse and meteorological data. *Atmospheric*
569 *Environment* **1986**, *20*, 949–964.
- 570 (35) Harris, E.; Sinha, B.; van Pinxteren, D.; Tilgner, A.; Fomba, K. W.; Schneider, J.; Roth,
571 A.; Gnauk, T.; Fahlbusch, B.; Mertes, S.; Lee, T.; Collett J.; Foley, S.; Borrmann, S.; Hoppe,
572 P.; Herrmann, H. Enhanced Role of Transition Metal Ion Catalysis During In-Cloud
573 Oxidation of SO₂. *Science* **2013**, *340*, 727–730.
- 574 (36) Welz, O.; Savee, J. D.; Osborn, D. L.; Vasu, S. S.; Percival, C. J.; Shallcross, D. E.;
575 Taatjes, C. A. Direct Kinetic Measurements of Criegee Intermediate (CH₂OO) Formed by
576 Reaction of CH₂I with O₂. *Science* **2012**, *335*, 204–207.
- 577 (37) Hobbs, P. V.; Radke, L. F.; Lyons, J. H.; Ferek, R. J.; Coffman, D. J.; Casadevall, T. J.
578 Airborne measurements of particle and gas emissions from the 1990 volcanic eruptions of
579 Mount Redoubt. *J. Geophys. Res. Atmos.* **1991**, *96*, 18735–18752.
- 580 (38) Martin, R. S.; Sawyer, G. M.; Spampinato, L.; Salerno, G. G.; Ramirez, C.; Ilyinskaya,
581 E.; Witt, M. L. I.; Mather, T. A.; Watson, I. M.; Phillips, J. C.; Oppenheimer, C. A total
582 volatile inventory for Masaya Volcano, Nicaragua. *J. Geophys. Res.* **2010**, *115*, B09215.
- 583 (39) Saunders, S. M.; Jenkin, M. E.; Derwent, R. G.; Pilling, M. J. Protocol for the
584 development of the Master Chemical Mechanism, MCM v3 (Part A): tropospheric
585 degradation of non-aromatic volatile organic compounds. *Atmos. Chem. Phys.* **2003**, *3*, 161–
586 180.
- 587 (40) Atkinson, R.; Baulch, D. L.; Cox, R. A.; Crowley, J. N.; Hampson, R. F.; Hynes, R. G.;
588 Jenkin, M. E.; Rossi, M. J.; Troe, J. Evaluated kinetic and photochemical data for
589 atmospheric chemistry: Volume I-gas phase reactions of O_x, HO_x, NO_x and SO_x species.

- 590 *Atmos. Chem. Phys.* **2004**, *4*, 1461–1738.
- 591 (41) Stone, D.; Whalley, L. K.; Heard, D. E. Tropospheric OH and HO₂ radicals: field
592 measurements and model comparisons. *Chem. Soc. Rev.* **2012**, *41*, 6348.
- 593 (42) Hobbs, P. V.; Tuell, J. P.; Hegg, D. A.; Radke, L. F.; Eltgroth, M. W. Particles and gases
594 in the emissions from the 1980–1981 volcanic eruptions of Mt. St. Helens. *J. Geophys. Res.*
595 *Atmos.* **1982**, *87*, 11062–11086.
- 596 (43) Martin, D.; Ardouin, B.; Bergametti, G.; Carbonnelle, J.; Faivre Pierret, R.; Lambert, G.;
597 Le Cloarec, M. F.; Sennequier, G. Geochemistry of sulfur in Mount Etna plume. *J. Geophys.*
598 *Res. Atmos.* **2007**, *91*, 12249–12254.
- 599 (44) Krueger, A. J.; Schnetzler, C. C.; Walter, L. S. The December 1981 eruption of
600 Nyamuragira volcano (Zaire), and the origin of the “mystery cloud” of early 1982. *J.*
601 *Geophys. Res. Atmos.* **1996**, *101*, 15191–15196.
- 602 (45) Porter, J. N.; Horton, K. A.; Mougini-Mark, P. J.; Lienert, B.; Sharma, S. K.; Lau, E.;
603 Sutton, A. J.; Elias, T.; Oppenheimer, C. Sun photometer and lidar measurements of the
604 plume from the Hawaii Kilauea Volcano Pu'u O'o vent: Aerosol flux and SO₂ lifetime.
605 *Geophys. Res. Lett.* **2002**, *29*, 30-1–30-4.
- 606 (46) Bluth, G. J. S.; Carn, S. A. Exceptional sulfur degassing from Nyamuragira volcano,
607 1979–2005. **2008**, 1–20.
- 608 (47) Rodríguez, L. A.; Watson, I. M.; Edmonds, M.; Ryan, G.; Hards, V.; Oppenheimer, C.
609 M. M.; Bluth, G. J. S. SO₂ loss rates in the plume emitted by Soufrière Hills volcano,
610 Montserrat. *Journal of Volcanology and Geothermal Research* **2008**, *173*, 135–147.
- 611 (48) McCormick, B. T.; Herzog, M.; Yang, J.; Edmonds, M.; Mather, T. A.; Carn, S. A.;
612 Hidalgo, S.; Langmann, B. A comparison of satellite- and ground- based measurements of
613 SO₂ emissions from Tungurahua volcano, Ecuador. *J. Geophys. Res. Atmos.* **2014**, *119*,
614 4264–4285..
- 615 (49) Oppenheimer, C.; Francis, P.; Stix, J. Depletion rates of sulfur dioxide in tropospheric
616 volcanic plumes. *Geophys. Res. Lett.* **1998**, *25*, 2671–2674.
- 617 (50) Clegg, S. L.; Brimblecombe, P.; Wexler, A. S. Thermodynamic model of the system H⁺-
618 NH₄⁺-SO₄²⁻-NO₃⁻-H₂O at tropospheric temperatures. *J. Phys. Chem. A* **1998**, *102*, 2155–2171.
- 619 (51) Zhang, Q.; Jimenez, J. L.; Worsnop, D. R.; Canagaratna, M. A Case Study of Urban
620 Particle Acidity and Its Influence on Secondary Organic Aerosol. *Environmental Science &*
621 *Technology* **2007**, *41*, 3213–3219.
- 622 (52) Pathak, R. K.; Yao, X.; Lau, A. K. H.; Chan, C. K. Acidity and concentrations of ionic
623 species of PM_{2.5} in Hong Kong. *Atmospheric Environment* **2003**, *37*, 1113–1124.

624

625

626 TOC/abstract graphic.



627

628

629 Image from NASA, <http://earthobservatory.nasa.gov/IOTD/view.php?id=2449>

630 Satellite images from NASA are public domain; please see

631 http://www.nasa.gov/audience/formedia/features/MP_Photo_Guidelines.html